Geological Materials Research
Volume 4
Number 2
August 12, 2002

Compositional asymmetry in replacement tourmaline – An example from the Tauern Window, Eastern Alps

Darrell J. Henry[1], Barbara L. Dutrow[2] and Jane Selverstone[3]

[1, 2]Department of Geology and Geophysics, Louisiana State University, Baton Rouge, Louisiana 70808, USA [1]<henry@geol.lsu.edu>, [2]<dutrow@geol.lsu.edu>, [3]Department of Earth and Planetary Sciences, University of New Mexico, Albuquerque, New Mexico 87131, USA [3]<selver@unm.edu >

Abstract

Tourmaline, partially replacing pre-existing tourmaline from a tectonically-dismembered tourmalinite vein, has developed distinctive compositional asymmetry that reflects influx of reactive fluids. The tourmalinite clast, enclosed in a quartzite from the Tauern Window, Eastern Alps, experienced a clockwise P-T-t path with maximal burial depths of 35-40 km (10-11 kbar), peak temperatures of ~550°C and major deformation preceding peak thermal conditions. The primary tourmaline of the tourmalinite clast, generation-1, is texturally and compositionally heterogeneous, ranging from schorl to dravite [Mg / (Mg + Fe) = 0.27 - 0.61] with highly-variable Al consistent with combinations of the $^{X}\square Al(NaR)_{-1}$ and $AlO(R(OH))_{-1}$ exchange vectors, where $^{X}\square$ represents X-site vacancy and R is Fe^{2+} + Mn + Mg. Generation-2 tourmaline is manifest as distinctive compositionally-asymmetric bands of colorless foitite (zone 1) and blue schorl (zone 2) replacing generation-1 tourmaline. Replacement takes place along a scalloped margin and advances preferentially towards the analogous pole (-c) of generation-1 tourmaline. The two zones of generation-2 range from foitite to schorl with a restricted ratio of Mg / (Mg + Fe) of 0.32 - 0.41, but with variable $^{X}\square$, Al, Na and R predominantly reflecting $^{X}\square Al(NaR)_{-1}$. Post-deformational generation-3 tourmaline ranges from schorl to foitite and partially pseudomorphs generations-1 and -2 tourmaline. Deformation and fracturing of primary tourmaline (generation 1) from the tourmalinite clast provided access to reactive fluids with adequate chemical affinity to produce partial tourmaline replacement. It is likely that the reactive fluid was a neutral-to-alkaline aqueous fluid phase with relatively low Na contents.

Keywords: tourmaline, replacement, fluids, Tauern Window, Alps.

Introduction

Tourmaline has a variety of polar characteristics reflecting its non-centrosymmetric nature. All of the apices of the SiO_4 tetrahedra point toward the negative end of the c axis of tourmaline to produce the crystallographic polar asymmetry (Barton, 1969; Dietrich, 1985). Morphologically, the polar nature of tourmaline is commonly manifested by hemimorphic development of distinctly different pyramidal and pedial faces and forms at the respective positive (antilogous or +c) and negative (analogous or -c) ends of the c axis (Dietrich, 1985; Henry and Dutrow, 1996). The non-centrosymmetry results in piezoelectric and pyroelectric responses to changing stresses and temperature, with the intensity of the pyroelectric response being composition-dependent (Hawkins et al., 1995). In etching experiments, deeper etch pits develop at the +c end relative to the -c end of tourmaline, i.e. the rate of solution is greater in the -c direction (Dietrich, 1985). In diagenetic and epigenetic environments, tourmaline nucleating on detrital grains grows at a greater rate at the +c end of the crystal. Tourmaline developed in low-to-medium grade metamorphic environments commonly displays a style of compositional asymmetry in

which there are distinct compositional differences at the +c end relative to –c end of the crystal (e.g. Henry and Dutrow, 1992, 1996; Sperlich et al., 1996; Henry et al., 1999). This style of compositional asymmetry, termed compositional polarity, is essentially a manifestation of chemical sector zoning because concurrently-crystallizing growth sectors in a given crystal develop disparate compositions (Henry et al, 1999).

Tourmaline is stable over a wide range of temperatures (near-surface to granulite-facies conditions), pressures (near-surface to >60 kbar), bulk compositions and mineral assemblages (Henry and Guidotti, 1985; Henry and Dutrow, 1996; Werding and Schreyer, 1996). If tourmaline does break down within these general thermal and baric conditions, the primary controlling factor for its stability is the composition of the fluid phase with which it interacts. This fluid phase may range from being rock-buffered to externally-controlled. Nonetheless, tourmaline becomes unstable when the fluid either becomes alkaline or the activities of ions in aqueous fluids, especially B^{3+}, Na^{+}, Fe^{2+}, Fe^{3+}, Mg^{2+}, Al^{3+}, destabilize tourmaline relative to other minerals (Morgan and London, 1989; London et al., 1996; Dutrow et al., 1999; London, 1999). In geologic environments in which the fluid phase is highly reactive and mutable, any pre-existing tourmaline may be susceptible to destabilization, breakdown and/or replacement. This feature is most commonly observed in environments where there is an influx of reactive fluids that may be associated with fracturing events such as quartz veining or pegmatite pocket breach (e.g. Pezzotta et al., 1996; Srein et al., 1997; Novák, 1998; Aurisicchio et al., 1999; Dutrow and Henry, 2000).

This paper describes a style of compositional asymmetry associated with tourmaline replacement phenomena that is distinctly different than simple compositional polarity. The compositionally-asymmetric tourmaline is a replacement phase typically developed proximal to fractures in primary tourmaline from a tectonically-dismembered tourmalinite vein in a quartzite located in the Tauern Window, Eastern Alps. A combination of backscattered electron and cathodoluminescent imaging, together with detailed mineral chemistry, establishes the compositional nature of the original and replacement tourmaline in the tourmalinite clast, and relates the generations of tourmaline growth to the deformational, metamorphic, and fluid evolution of the sample.

Geologic and Metamorphic Setting

The Tauern Window in the Eastern Alps is a large tectonic window that exposes deep-seated crustal and neo-Tethys oceanic rocks beneath the overthrust units of the Austroalpine nappe sequence (Selverstone et al., 1984, 1991; Selverstone and Munoz, 1987; von Blanckenberg et al., 1989; Selverstone, 1993). Thrusting occurred during the Alpine orogeny in latest Cretaceous through mid-Tertiary time, and was followed by extensional and erosional unroofing of the rocks within the window (e.g. Smith and Woodcock, 1982). These rocks are subdivided into three lithotectonic packages: the Zentralgneis, the Lower Schieferhülle series, and the Upper Schieferhülle series. The Zentralgneis is composed of pre-Alpine plutonic rocks that locally intrude the Paleozoic portions of the Lower Schieferhülle (Morteani, 1974). The Lower Schieferhülle contains both Permo-Carboniferous graphitic schists and metavolcanic rocks, and also a younger cover sequence of Permo-Triassic metaconglomerates, quartzites, and schists. The Upper Schieferhülle contains greenstones, marbles and pelitic schists originally derived from the floor of the neo-Tethys ocean basin.

The tourmalinite sample was collected from a 25-m wide horizon of quartzite in the cover sequence of the Lower Schieferhülle series in the region of the Pfitsch Pass (Pfitscher Joch) on the Austrian/Italian border. The quartzite and crosscutting tourmalinite veins are folded into a tight synform, and have also been strongly tectonized within the 1 km wide, subvertical Greiner shear zone, a structure considered to be of Alpine age (Selverstone, 1993). The quartzite is bordered to the north by a polymict metaconglomerate containing clasts of Zentralgneis and serpentinite, and to the south by calcite-bearing biotite-epidote mica schists and gneisses (Selverstone et al., 1984, 1991; Selverstone and Munoz, 1987; Selverstone, 1993; Morteani and Ackermand, 1996). The quartzite host contains a variety of unusual aluminum phosphate minerals, such as lazulite, crandallite, and bearthite, and has been interpreted as having originated from a sabkha-like sediment (Morteani and Ackermand, 1996). Similar phosphate-rich quartzites, found along the length of the Penninic Alps, are Permo-Triassic in depositional age (summarized in Morteani and Ackermand, 1996), and a similar age seems likely for the protolith of the quartzite studied here.

Quartz and quartz + tourmaline veins crosscut the quartzite and adjacent rocks, and are isoclinally folded. In many cases, shearing along the foliation, parallel to the axial planes of these folds, has dismembered the veins and produced elliptical quartz ± tourmaline clasts that are entirely surrounded by the quartzite matrix (Fig. 1). Vein emplacement clearly postdated Permo-Triassic deposition of the quartzite protolith, and predated shearing and peak thermal Alpine metamorphism. The sample studied here represents a clast derived from one of the dismembered tourmalinite veins and was collected approximately 500

Figure 1. Quartzite from the Lower Schieferhülle series. The highly-deformed tourmaline-quartz vein cuts the quartzite. The upper part of the image shows a more weathered portion of the sheared quartzite. A 2-cm hand lens is shown for scale.

m along strike from the lazulite-bearing quartzite samples described by Morteani and Ackermand (1996).

During the Alpine orogeny, the Lower Schieferhülle series followed a clockwise P-T path that reached a maximum pressure of 10-11 kbar at ~520˚C followed by a maximum temperature of ~550˚C (T_{max}) and near-isothermal decompression at 7-8 kbar (Selverstone et al., 1984). The pressure maximum may have been attained as early as 55 Ma, and the thermal maximum occurred at 30 ± 1 Ma in this area (Christensen et al., 1994; Selverstone, 1993). Most of the deformation and the dismemberment of the tourmaline-quartz veins within the Greiner shear zone occurred prior to attainment of the Oligocene (30 Ma) thermal peak (T_{max}) as indicated by postkinematic porphyroblast growth in the Lower Schieferhülle (Selverstone, 1985, 1993).

Sample Description

The sample is a strongly deformed quartzite with a relatively large, oblong clast of banded tourmalinite (15 mm by 8 mm), derived from a dismembered tourmaline + quartz vein. The long dimension of the clast is subparallel to the axial planar foliation and to the tourmalinite banding as defined primarily by variable proportions of tourmaline and quartz. The foliation of the quartzite, generally marked by aligned muscovite, wraps around the tourmalinite clast.

The host quartzite has an assemblage of quartz + muscovite + kyanite + lazulite + ilmenite + rutile + gray-blue tourmaline + apatite + zircon + chalcopyrite. Augen-shaped, partially-recrystallized quartz grains (up to 4 mm by 2.5 mm) are elongate parallel to the foliation defined by muscovite. Sheaths of muscovite partially wrap around the deformed and recrystallized quartz. Minor amounts of optically unzoned gray-blue tourmaline (10-50 μm in cross-section) locally develop at the margin of the tourmalinite clast or partially replace portions of the aligned muscovite defining the foliation. Ilmenite is most commonly interleaved with the muscovite, but is locally dispersed in quartz grains. Kyanite and pale blue lazulite overprint the foliation, contain inclusions of quartz, ilmenite, gray-blue tourmaline, zircon and apatite and post-date the general deformational features of the quartzite. However, Morteani and Ackermand (1996) note that the interior portions of many lazulite grains in quartzites from the same area also developed prior to deformation and recrystallization, and probably initially crystallized earlier in the metamorphic history of the quartzites.

Tourmaline-rich and quartz-rich layers, 1-3 mm thick, comprise the tourmalinite clast. Tourmaline-rich bands contain up to 75% tourmaline and quartz-rich bands contain <10% tourmaline. The mineral assemblage of the clast is quartz + tourmaline + muscovite + apatite + ilmenite + rutile + zircon + chalcopyrite. Quartz (200-1000 μm) locally exhibits a granoblastic texture within the clast. Apatite is locally plentiful (≤2%), relatively coarse (≤200 μm in length) and is included in the tourmaline as well as in the matrix. Small, rounded grains of zircon (<20 μm) as well as grains of chalcopyrite (<30 μm), ilmenite (50-200 μm) and rutile (30-50 μm) are also found as inclusions in tourmaline and in the matrix. Locally, rutile partially replaces ilmenite both within tourmaline and in the matrix. Muscovite exhibits a random orientation within the clast indicating that the extensive penetrative deformation did not strongly affect the interior of the tourmalinite clast. There are three generations of tourmaline within or near the tourmalinite clast: (a) Green-to-brown generation-1 tourmaline that occurs in the original tourmalinite vein, (b) Blue-to-colorless color-zoned generation-2 tourmaline bands associated with crosscutting fractures within, or at the margins of, generation-1 tourmaline and (c) Gray-blue and pale green-blue generation-3 tourmaline crystals developed at, or near, the margin of the clast.

Generation-1 tourmaline preserves much of the primary textural and optical growth characteristics of the tourmaline crystallized in the original tourmalinite vein (Figs. 2, 3, 4). Tourmaline grains are subhedral with dimensions of 50-800 μm in cross-section perpendicular to the c-axis and 250-2500 μm parallel to the c-axis, i.e. generally with length/width ratios of 3-5. The long dimensions of the tourmaline crystals are typically within the planes of layering in the tourmaline clast, but the tourmaline crystals do not exhibit significant lineation

within those planes. Optically, generation-1 tourmaline has a complex, heterogeneous zoning pattern with the interior of the tourmaline grains having patches or bands with maximum absorption colors of pale-to-medium green and brown-green generally surrounded by irregular zones or oscillatory bands with a dark gray-green maximum absorption colors (Fig. 2). In some areas the dark gray-green bands crosscut earlier growth features in the brown-green and green zones. There are rare pyramidal faces, and oscillatory zones parallel to the pyramidal faces, with poorly-developed pedial forms at the opposite pole that aid in defining the orientation of the +c vs. -c end of the crystal (cf. Dietrich, 1985). Some of the generation-1 tourmaline grains also contain isolated, primary fluid inclusions with euhedral negative crystal forms which also help establish the relative polarity of the tourmaline, with the pointed end (mostly pyramidal forms) oriented toward the +c end and the flat end (pedial forms) oriented toward the -c end of the crystals (Fig. 3). The primary fluid inclusions are typically three-phase with a volumetrically-dominant CO_2 liquid + vapor and lesser amounts of aqueous fluid (Fig. 3).

Generation-2 tourmaline occurs as distinctive, asymmetrically color-zoned (colorless-to-blue) bands of tourmaline that crosscut all primary growth features developed in generation-1 tourmaline (Figs. 2-4). Although generation-2 tourmaline bands are found on the margins of some generation-1 tourmaline grains, generation-2 tourmaline bands are most commonly associated with a series of crosscutting straight-to-curvilinear fractures oriented roughly perpendicular to the c-axis of generation-1 tourmaline. The fractures have little or no displacement but, where displaced, quartz fills the separated fractures (Fig. 2). The 10-80 μm color-zoned bands of generation-2 tourmaline contain a 5-20 μm

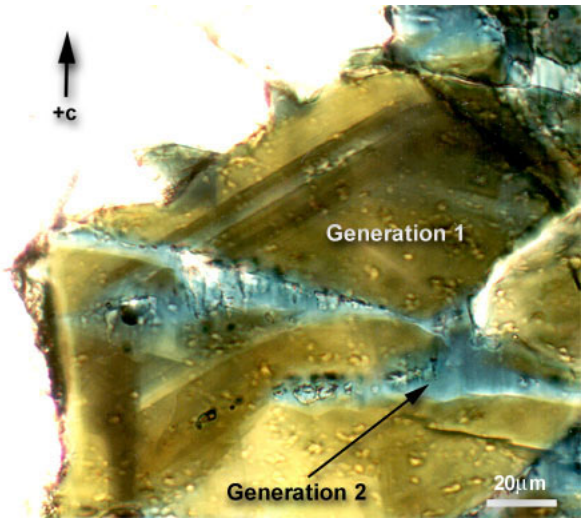

Figure 2. Photomicrograph of generation-1 tourmaline developed during primary tourmalinite formation and crosscut by generation-2 tourmaline. Oscillatory zoning in generation-1 tourmaline is parallel to the pyramidal faces. Crosscutting generation-2 tourmaline bands exhibit asymmetric color zonation from a blue band (zone 2) to a thin colorless band (zone 1) in the –c direction of the crystallographic c-axis i.e. analogous pole. The original fracture is commonly decorated with quartz and fluid inclusions along the upper boundary of the generation-2 tourmaline band. The photomicrograph is in plane-polarized light that is oriented to produce maximal optical absorption in the tourmaline.

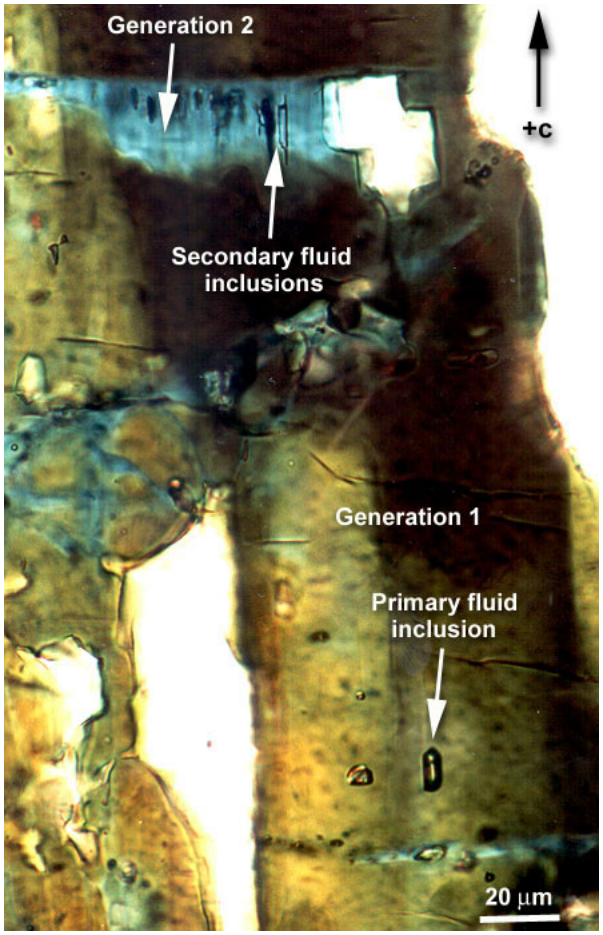

Figure 3. Photomicrograph of generation-1 tourmaline with isolated three-phase primary fluid inclusions exhibiting negative crystal form. The pyramidal form at the upper end of the inclusion indicates the +c end is toward the top of the image. Bands of blue (zone 2) generation-2 tourmaline cut and replace generation-1 color-zoned regions. There is a very thin (1-3 mm) band of colorless (zone 1) generation-2 tourmaline that marks a scalloped interface with the generation-1 tourmaline at the lower part of the generation-2 bands. Secondary fluid inclusions are concentrated nearest the upper part of the generation-2 band that marks the location of the original fracture. The photomicrograph is in plane-polarized light that is oriented to produce maximal optical absorption in the tourmaline.

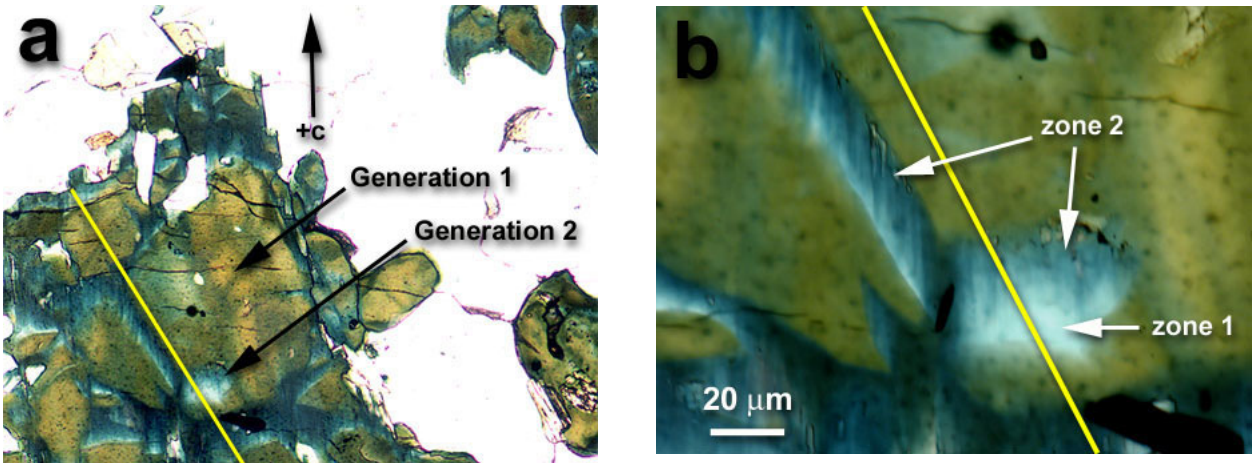

Figure 4. Photomicrographs of bands of generation-2 tourmaline cutting heterogeneously-zoned generation-1 tourmaline. (a) Large tourmaline crystal oriented approximately parallel to the c-axis of the crystal, with the antilogous pole (+c end) of the crystal toward the top of the image. The generation-2 bands are asymmetrically color-zoned such that the colorless zone-1 tourmaline is always found at the bottom of the band, in the –c direction, and the blue zone-2 tourmaline is always found at the top of the band. Generation-2 tourmaline is in optical continuity with the host generation-1 tourmaline. The yellow line represents the trace of a detailed microprobe traverse shown in Figure 7. (b) Enlarged portion of generation-2 tourmaline bands in generation-1 tourmaline host. The blue zone-2 tourmaline has an acicular shape and is intergrown with the colorless zone-1 tourmaline. A backscattered electron image of portions of this area is presented in Figure 6.

wide zone (zone-1) of colorless tourmaline that is intergrown with a thicker zone (zone-2) of blue acicular tourmaline crystals (Fig 4). The blue zone-2 tourmaline band is associated with the fractures, and commonly contains small rutile crystals and abundant fluid inclusions concentrated proximal to the fracture. At the opposite side of the generation-2 band, the band of zone-1 colorless tourmaline exhibits a rounded and/or scalloped interface with the host generation-1 tourmaline. The original growth patterns of the generation-1 tourmaline do not match across the generation-2 bands indicating that this generation of tourmaline must have formed by replacement rather than infilling of a separated fracture (cf. Craig and Vaughan, 1994). All generation-2 bands within a single grain are optically-continuous with the host generation-1 tourmaline, and are color-zoned in the same manner and direction, implying a crystallographic control on replacement zoning patterns (Fig. 4). Based on the orientation of prismatic vs. pedial faces in the generation-1 tourmaline and the negative crystal forms exhibited by some primary fluid inclusions, asymmetrically-zoned generation-2 tourmaline bands progressively replaced generation-1 tourmaline toward the analogous pole (-c) of the tourmaline crystals.

Generation-3 tourmaline develops at, or near, the margin of the tourmalinite clast as post-deformational crystals. There are two varieties of generation-3 tourmaline, each having distinct characteristics. A gray-blue variety of generation-3 tourmaline locally replaces portions of generations-1 and -2 tourmaline, crosscutting pre-existing growth features (Fig. 5). This variety of generation-3 tourmaline also partially pseudomorphs previously-aligned muscovite, commonly preserving some of the muscovite textural features within the generation-3 tourmaline. The second variety of generation-3 tourmaline is represented by separate fine-grained, subhedral pale green-blue acicular crystals (10-30 μm in cross-section) that are located in the quartz matrix or nucleate at the +c end of a larger generation-1 crystal. Because this second variety of tourmaline is developed only near the margin of the clast rather than throughout the clast, it is considered to be associated with the third stage of tourmaline development. Both varieties of generation-3 tourmaline exhibit minor optical zoning.

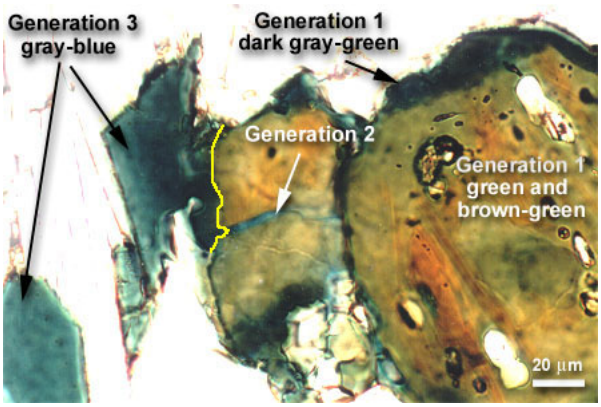

Figure 5. Photomicrograph of gray-blue generation-3 tourmaline crystallizing in the muscovite-rich margin of the clast and replacing early generation tourmaline. The yellow line represents the interface between generation-3 tourmaline and earlier generation tourmaline. The interior of the generation-1 tourmaline displays an irregular patchy zoning of green and brown-green zones partially replaced by a rim of dark gray-green generation-1 tourmaline.

Imaging and analytical procedures

Imaging

Combinations of optical, backscattered electron (BSE) and scanning electron microscope cathodoluminescence (SEM-CL) images were used to establish the relative growth, fracturing and replacement features of the three generations of tourmaline. The three generations of tourmaline exhibit optically distinct absorption colors and/or textures. BSE images, obtained with a JEOL 733 electron microprobe and a JEOL 860 SEM at Louisiana State University, reveal detailed growth and reaction features, and serve as a base map for quantitative analyses. Color SEM-CL imaging is useful for establishing the growth and fracture history of several minerals, particularly quartz. The color SEM-CL images were obtained with an Oxford Instruments PanaCL F system attached to the JEOL 860 SEM. CL light is collected with a parabolic mirror and color is attained by sequentially inserting a red, green and blue filter to obtain three separate CL images. The three images are then recombined using an image-processing program to reconstruct the fully integrated color image.

Electron microprobe analysis and tourmaline crystal chemical constraints

Tourmaline and associated minerals were quantitatively analyzed by wavelength-dispersive spectrometry (WDS) using the automated JEOL 733 electron microprobe at LSU. WDS analyses were performed using an accelerating potential of 15 kV and a beam current of 5-10 nA with a 1-2 μm focussed electron beam. Well-characterized synthetic and natural silicates were used as standards, and the data were corrected on-line using a ZAF correction procedure. On the basis of replicate analyses of several secondary standards, analytical precision associated with counting statistics for selected oxides is estimated to be ± 0.21% SiO_2, ± 0.13% Al_2O_3, ± 0.06% FeO, ± 0.11% MgO, ± 0.02% CaO and ± 0.03% Na_2O.

The most appropriate normalization procedures for tourmaline were carefully considered. The general formula for tourmaline can be expressed as $XY_3Z_6(T_6O_{18})(BO_3)_3V_3W$ (Hawthorne and Henry, 1999). The X site contains Na, Ca, K, and vacancies ($^X\square$); the two distinct octahedral sites, Y and Z, are occupied by a variety of divalent, trivalent and tetravalent cations; and Si, with lesser Al, dominates the tetrahedral T site. The triangular B site is occupied exclusively by B. There are two distinct anion sites that can contain OH^- and/or O^{2-}, the V and W sites. Furthermore, F^- is found exclusively on the W site, and O^{2-} also tends to partition into this site. Tourmaline formulae were normalized on the basis of 15 cations exclusive of Na, Ca and K, i.e., assuming no vacancies at the tetrahedral or octahedral sites and insignificant Li content (Henry and Dutrow, 1996; Henry et al., 1999). This cation normalization procedure has the advantage of being independent of oxidation states of transition elements and H contents in tourmaline, as long as the major cations are measured (Henry and Dutrow, 1996). Insignificant amounts of Li in tourmaline are probable because Li tends to strongly partition into any coexisting muscovite relative to tourmaline (Dutrow et al., 1986; Henry and Dutrow, 1996). The amount of B_2O_3 necessary to produce three B cations in the structural formula was calculated from stoichiometric constraints. Because of the weak pleochroism of the tourmaline and the general antithetic nature of Fe with the other octahedral divalent cations, it is assumed that the Fe is essentially all Fe^{2+} (see discussion below). Consequently, charge-balance constraints could be used to estimate the amount of H and O associated with the V and W anion sites in the structural formula, although this calculation is subject to significant amounts of uncertainty (Henry and Dutrow, 1996, 2001; Dutrow and Henry, 2000). The structural formulae of the tourmaline species considered significant in this sample are given in Table 1.

Results

SEM-CL imaging

Color SEM-CL imaging reveals several notable features that relate to the evolution of the tourmalinite clast. Zircon, apatite and quartz exhibit distinctive cathodoluminescence, but other minerals in the sample are nonluminescent (Fig. 6). Zircon luminesces a relatively uniform bright blue-white and is easily visible

Table 1. Structural formulae for notable tourmaline species associated with tourmalinite.

Species	(X)	(Y_3)	(Z_6)	T_6O_{18}	$(BO_3)_3$	$(V)_3$	(W)
Schorl	Na	$Fe^{2+}{}_3$	Al_6	Si_6O_{18}	$(BO_3)_3$	$(OH)_3$	(OH)
Dravite	Na	Mg_3	Al_6	Si_6O_{18}	$(BO_3)_3$	$(OH)_3$	(OH)
Foitite[1]	□	$Fe^{2+}{}_2$ Al	Al_6	Si_6O_{18}	$(BO_3)_3$	$(OH)_3$	(OH)
Magnesiofoitite	□	Mg_2 Al	Al_6	Si_6O_{18}	$(BO_3)_3$	$(OH)_3$	(OH)

[1]Species formula modified from the original formula by Hawthorne and Henry (1999)

throughout the sample. Apatite has a bright yellow CL response with no apparent luminescent zoning. There are two varieties of luminescence in quartz. (1) Isolated quartz inclusions in generation-1 tourmaline exhibit blue luminescence, most likely due to elevated Ti and/or Al contents in quartz (e.g. Zinkernagel, 1978; Matter and Ramseyer, 1985; Perny et al., 1992; Bruhn et al., 1996). (2) Matrix quartz and quartz in fractures within tourmaline luminesce red, likely due elevated Fe^{3+} and/or defect-centers related to OH^- incorporation (e.g. Bruhn et al., 1996). CL of the matrix quartz is relatively uniform with no indication of a fracture system that extends from the fractures preserved in the generation-1 tourmaline. However, there are grain-to-grain variations in the red/blue intensity that are likely the result of differences in crystallographic orientations of the matrix quartz (e.g. Walderhaug and Rykkje, 2000). In addition, the quartz found in fractures associated with the development of generation-2 tourmaline also luminesces red, similar to that of the matrix quartz. Thus, the quartz had likely annealed after the deformation that fractured the generation-1 tourmaline in the clast. Morteani and Ackermand (1996) made a similar observation in that lazulite preserves secondary fluid inclusions that stop at the interface with quartz where the quartz has apparently undergone polygonal recrystallization.

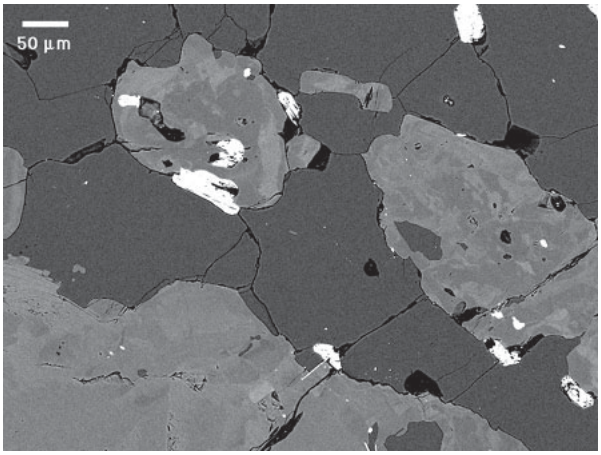

Figure 6. BSE and SEM-CL (rollover) images of portions of the tourmalinite clast. The BSE image allows differentiation of quartz (dark gray), tourmaline (medium gray, patchy) and apatite + zircon (white). SEM-CL allows further mineralogical distinctions due to the variable luminescent characteristics of quartz, zircon and apatite. Zircon luminesces blue-white and is included in tourmaline and the quartz matrix. Apatite luminesces green-yellow. Quartz exhibits two types of luminescence: blue-luminescing generation-1 quartz developed as isolated inclusions in generation-1 tourmaline and red-luminescing generation-2 quartz that develops in the recrystallized matrix as well as in the quartz associated with fractures that develop the generation-2 tourmaline. Tourmaline is non-luminescent.

Mineral chemistry of associated minerals

The lazulite in the quartzite is essentially a binary solution between lazulite $[MgAl_2(PO_4)_2(OH)_2]$ and scorzalite $[FeAl_2(PO_4)_2(OH)_2]$ with an Mg/(Mg+Fe) value of 0.75 (Table 2). Most other substituents are minor with <0.1 wt% of the other oxides. The 0.22 wt% F is slightly higher than other trace constituents, but still a minor substituent. Based on charge balance calculations, the proportion of Fe as Fe^{3+} is also considered minor. Near-binary solid solutions of the lazulite have also been found in metaquartzites from a nearby Lower Schieferhülle locality of the Tauern Window (Morteani and Ackermand, 1996).

Representative analyses of muscovite crystals that occur as oriented laths defining the foliation of the quartzite, as randomly-oriented laths in the matrix of the tourmalinite clast, and as inclusions in generation-2 tourmaline at the margins of generation-1 tourmaline are compositionally similar (Table 2). This implies that chemical equilibrium was generally attained among the different textural types of muscovite at, or near, the peak of thermal metamorphism. The muscovite is moderately paragonitic with Na / (Na + K + Ca) values of 0.146 - 0.149. In contrast to the lazulite, the muscovite has low Mg / (Mg + Fe) values of 0.10-0.11. Interestingly, Si values of 3.037 - 3.053 atoms per formula unit (apfu) and (Fe + Mn + Mg) values of 0.167 - 0.178 apfu are low relative to more celadonitic white micas from other Tauern Window rocks (e.g. Kurz et al., 1998).

Tourmaline chemistry, zoning and replacement textures

A detailed traverse across a tourmaline crystal oriented roughly parallel to its c-axis establishes the major

Table 2. Representative compositions of associated minerals in tourmalinite.

	Muscovite			Lazulite
Occurrence	**Host rock foliation ms**	**Tourmalinite matrix**	**Tourmalinite tur inclusion**	**Porphyroblast**
# of analyses	3.00	2.00	1.00	3.00
SiO_2	44.91	44.92	45.01	0.08
P_2O_5	n.d.	n.d.	n.d.	45.97
Al_2O_3	35.51	35.01	35.39	33.08
TiO_2	0.15	0.21	0.20	0.04
Cr_2O_3	0.01	0.00	0.02	0.00
FeO	2.66	2.62	2.79	5.95
MnO	0.02	0.00	0.04	0.03
MgO	0.17	0.18	0.19	9.84
CaO	0.00	0.00	0.00	0.00
BaO	0.14	0.14	0.14	n.d.
Na_2O	1.11	1.12	1.12	0.00
K_2O	9.75	9.75	9.94	0.01
F	0.00	0.02	0.10	0.22
Cl	0.00	0.01	0.00	n.d.
Total	94.43	93.98	94.95	95.22
Norm Basis	O=11	O=11	O=11	O=9
Si	3.04	3.05	3.04	0.00
P	-	-	-	1.99
^{IV}Al	0.96	0.95	0.96	-
^{VI}Al	1.87	1.86	1.85	2.00
Ti	0.01	0.01	0.01	0.00
Cr	0.00	0.00	0.00	0.00
Fe^{2+}	0.15	0.15	0.16	0.26
Mn	0.00	0.00	0.00	0.00
Mg	0.02	0.02	0.02	0.75
^{VI}total	2.04	2.03	2.04	-
Ca	0.00	0.00	0.00	0.00
Ba	0.00	0.00	0.00	-
Na	0.15	0.15	0.15	0.00
K	0.84	0.85	0.86	0.00
^{XII}total	0.99	1.00	1.01	-
F	0.00	0.00	0.02	0.04
Cl	0.00	0.00	0.00	-
Mg/(Mg+Fe)	0.10	0.11	0.11	0.75
Na/(Na+K+Ca)	0.15	0.15	0.15	-

compositional differences between generations-1 and -2 tourmaline (Fig. 7). Regions of generation-1 tourmaline are texturally and compositionally distinct from generation-2 tourmaline. Generation-1 tourmaline is compositionally heterogeneous, with the greatest variation being due to a roughly inverse relationship between Mg and Fe. There does not appear to be any systematic zonal distribution of the Mg-richer and Mg-poorer regions of generation-1 tourmaline. In contrast, generation-2 tourmaline exhibits a systematic compositional asymmetry. In the direction of the -c end, the colorless zone-1 margin of the generation-2 bands are enriched in Al and $^{X}\square$ at the expense of Fe, Mg and Na relative to the blue, zone-2 regions. A higher magnification BSE image of a portion of this grain illustrates the complex nature of the generation-2 replacement bands (Fig. 8). At the interface with the generation-1 tourmaline host, the colorless zone-1 (generation-2) tourmaline replaces generation-1 tourmaline along scalloped fronts. Variations in backscattered electron gray levels imply compositional

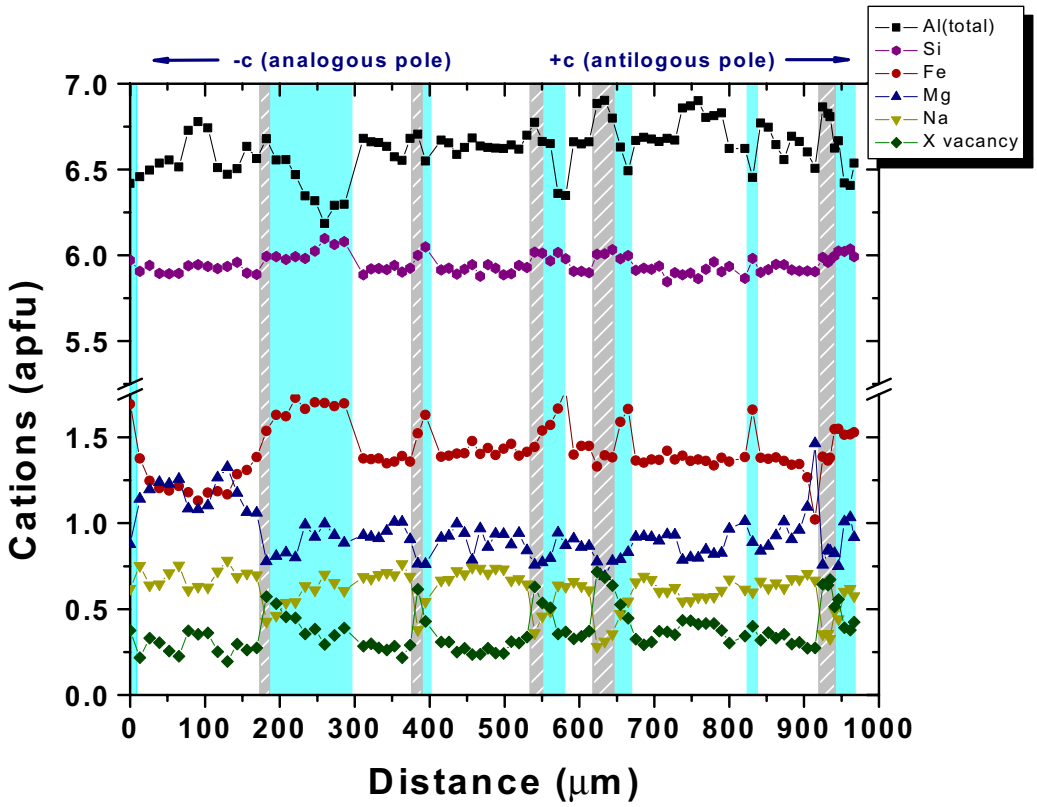

Figure 7. Detailed quantitative electron microprobe traverse of a tourmaline crystal displaying alternating zones of generation-1 tourmaline with bands of color-zoned generation-2 tourmaline (photomicrograph in Fig. 4). Generation-2 tourmaline exhibits compositional asymmetry with the colorless zone-1 tourmaline (gray hachured bands) being enriched in Al and $^{X}\square$ relative to the blue zone-2 tourmaline (solid light blue bands).

zoning is minor, but present in zone-1 (generation-2) tourmaline (Fig. 8). Zone-2 (generation-2) tourmaline develops as acicular blue tourmaline that nucleates at the fracture boundaries and intergrows with the colorless zone-1 (generation-2) tourmaline. Locally, the blue acicular zone-2 (generation-2) tourmaline appears to replace some of the textural features the colorless zone-1 (generation-2) tourmaline (Fig. 8).

Each tourmaline generation has heterogeneous color-zoned regions that generally have distinct compositional differences. Generation-1 tourmaline is divided into brown-green, dark gray-green, green and pale green color zones. On average, the pale green zones have a significantly higher X_{Mg} and the brown-green zones are slightly more aluminous than the other generation-1 color zones, but there is a considerable amount of overlap in compositions among most of the zones (Table 3). In the bands of generation-2 tourmaline the BSE zoning of the colorless zone-1 tourmaline and blue zone-2 tourmaline is discontinuous and compositional differences much more distinct (Table 4). The average change in composition from the colorless zone-1 tourmaline to that of the blue zone-2 tourmaline is ΔAl = -0.324, $\Delta^{X}\square$ = -0.193, ΔO =

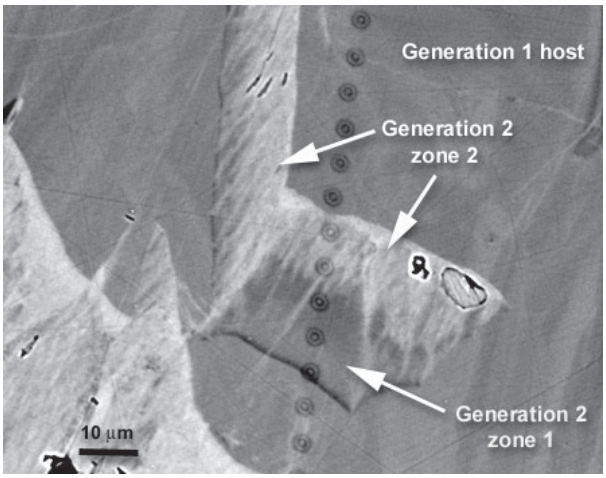

Figure 8. BSE image of generation-2 tourmaline replacing generation-1 tourmaline. The light gray acicular growths correspond to the blue generation-2 tourmaline (zone 2) and the darker-gray zones are colorless generation-2 tourmaline (zone 1). The 1-2 mm dark band at the scalloped replacement front is especially enriched in Al, Mg and $^{X}\square$. Note the lack of displacement of the heterogeneous growth features developed in the generation-1 tourmaline host. The spots are contamination spots from the microprobe traverse and correspond to the 600 to 725 μm positions (bottom to top) in Fig. 7.

Table 3. Average composition of each color zone within generation-1 tourmaline.

Generation	**1**	**1**	**1**	**1**
Color zone	**Brown-green**	**Dark gray-green**	**Green**	**Pale green**
# of analyses	25	11	4	24
B_2O_3[1] (wt%)	10.39 *(0.04)*[2]	10.28 *(0.03)*	10.28 *(0.04)*	10.44 *(0.07)*
SiO_2	35.31 *(0.22)*	34.79 *(0.28)*	34.73 *(0.17)*	35.56 *(0.19)*
Al_2O_3	33.79 *(0.49)*	33.07 *(0.58)*	32.93 *(0.10)*	33.19 *(0.64)*
TiO_2	0.81 *(0.17)*	1.05 *(0.15)*	0.97 *(0.06)*	0.81 *(0.22)*
Cr_2O_3	0.01 *(0.01)*	0.01 *(0.01)*	0.02 *(0.01)*	0.02 *(0.02)*
FeO	9.85 *(0.33)*	10.76 *(0.85)*	11.51 *(0.61)*	8.16 *(0.54)*
MnO	0.08 *(0.03)*	0.09 *(0.02)*	0.08 *(0.03)*	0.06 *(0.03)*
M	3.77 *(0.37)*	3.43 *(0.67)*	3.18 *(0.42)*	5.34 *(0.56)*
CaO	0.09 *(0.06)*	0.14 *(0.06)*	0.14 *(0.04)*	0.15 *(0.10)*
Na_2O	2.06 *(0.17)*	2.15 *(0.21)*	2.21 *(0.08)*	2.25 *(0.24)*
K_2O	0.04 *(0.01)*	0.04 *(0.01)*	0.04 *(0.02)*	0.04 *(0.01)*
F	0.06 *(0.06)*	0.03 *(0.03)*	0.08 *(0.05)*	0.10 *(0.10)*
Cl	0.00 *(0.01)*	0.01 *(0.01)*	0.01 *(0.01)*	0.00 *(0.01)*
TOTAL	96.28 *(0.39)*	95.85 *(0.31)*	96.15 *(0.29)*	96.12 *(0.53)*
O=F	0.02	0.01	0.03	0.04
TOTAL	96.26	95.84	96.12	96.08
Atomic proportions based on the sum of T+Z+Y cations normalized to 15 cations				
B[1]	3	3	3	3
Si	5.906 *(0.033)*	5.880 *(0.044)*	5.873 *(0.024)*	5.918 *(0.041)*
^{T}Al	0.094	0.120	0.127	0.082
^{Z}Al	6	6	6	6
^{Y}Al	0.567 *(0.092)*	0.468 *(0.121)*	0.435 *(0.020)*	0.428 *(0.117)*
Ti	0.102 *(0.022)*	0.133 *(0.018)*	0.123 *(0.008)*	0.101 *(0.028)*
Cr	0.002 *(0.001)*	0.002 *(0.002)*	0.002 *(0.002)*	0.003 *(0.002)*
Fe^{2+}	1.378 *(0.048)*	1.520 *(0.124)*	1.628 *(0.061)*	1.136 *(0.081)*
Mn	0.012 *(0.004)*	0.013 *(0.003)*	0.012 *(0.004)*	0.008 *(0.004)*
Mg	0.940 *(0.092)*	0.863 *(0.166)*	0.800 *(0.105)*	1.324 *(0.133)*
Ca	0.017 *(0.012)*	0.025 *(0.011)*	0.024 *(0.007)*	0.027 *(0.017)*
Na	0.668 *(0.054)*	0.706 *(0.069)*	0.724 *(0.027)*	0.728 *(0.079)*
K	0.008 *(0.002)*	0.009 *(0.003)*	0.009 *(0.004)*	0.008 *(0.003)*
$^{X}\square$[1]	0.307 *(0.058)*	0.261 *(0.067)*	0.243 *(0.025)*	0.237 *(0.079)*
F	0.030 *(0.029)*	0.015 *(0.019)*	0.044 *(0.029)*	0.052 *(0.053)*
Cl	0.001 *(0.001)*	0.001 *(0.002)*	0.001 *(0.002)*	0.001 *(0.001)*
OH[1]	3.581 *(0.067)*	3.604 *(0.042)*	3.618 *(0.021)*	3.606 *(0.077)*
O[1]	0.388 *(0.067)*	0.380 *(0.042)*	0.337 *(0.021)*	0.341 *(0.077)*
Mg/(Mg+Fe)	0.404 *(0.028)*	0.361 *(0.060)*	0.329 *(0.041)*	0.537 *(0.040)*

[1] Calculated using stoichiometric constraints (see Analytical Techniques).

[2] Numbers in parentheses are standard deviations of the mean (1σ). The standard deviation with ^{Y}Al is for total Al.

-0.093, ΔFe = +0.190, ΔMg = +0.115, ΔNa = +0.193 and ΔOH = +0.080 (Table 4). However, these averaged changes in composition in generation-2 tourmaline probably represent a minimum difference because of local intergrowth of zone-1 tourmaline and acicular zone-2 tourmaline resulting in some analytical overlap. The Ti, Na and Ca values of generation-2 tourmaline are significantly less than those of generation-1 tourmaline (Tables 3 and 4), with the elevated Ti levels accounting for the brown coloration commonly observed in generation-1 tourmaline (cf. Henry and Dutrow, 1996). Generation-3 tourmaline has relatively minor intragranular compositional zoning, but the gray-blue variety of tourmaline that partially replaces muscovite or tourmaline at the margin

Table 4. Average composition of each color zone within generations-2 and -3 tourmaline.

Generation	**2**	**2**	**3**	**3**
Color zone	**Colorless (zone 1)**	**Blue (zone 2)**	**Gray-blue**	**Pale green-blue**
# of analyses	10	24	12	4
B_2O_3[1] (wt%)	10.43 *(0.06)*	10.33 *(0.09)* [2]	10.34 *(0.07)*	10.52 *(0.03)*
SiO_2	36.02 *(0.21)*	35.73 *(0.26)*	35.25 *(0.22)*	36.32 *(0.12)*
Al_2O_3	34.48 *(0.52)*	32.53 *(0.83)*	33.20 *(0.37)*	34.19 *(0.38)*
TiO_2	0.04 *(0.02)*	0.13 *(0.09)*	0.30 *(0.07)*	0.18 *(0.09)*
Cr_2O_3	0.01 *(0.01)*	0.01 *(0.01)*	0.02 *(0.01)*	0.02 *(0.01)*
FeO	10.32 *(0.54)*	11.58 *(0.46)*	10.64 *(0.40)*	9.40 *(0.31)*
MnO	0.02 *(0.01)*	0.02 *(0.02)*	0.02 *(0.02)*	0.01 *(0.02)*
MgO	3.14 *(0.18)*	3.57 *(0.36)*	3.84 *(0.13)*	4.15 *(0.24)*
CaO	0.01 *(0.01)*	0.01 *(0.01)*	0.04 *(0.02)*	0.02 *(0.01)*
Na_2O	1.19 *(0.22)*	1.77 *(0.20)*	1.91 *(0.10)*	1.41 *(0.20)*
K_2O	0.01 *(0.01)*	0.01 *(0.02)*	0.04 *(0.02)*	0.01 *(0.01)*
F	0.01 *(0.01)*	0.04 *(0.04)*	0.04 *(0.03)*	0.02 *(0.03)*
Cl	0.00	0.00	0.00	0.00
TOTAL	95.68 *(0.64)*	95.73 *(0.72)*	95.64 *(0.67)*	96.25 *(0.29)*
O=F	0.01	0.02	0.02	0.01
TOTAL	95.52	95.72	95.86	96.24
Atomic proportions based on the sum of T + Z + Y cations normalized to 15 cations				
B[1]	3	3	3	3
Si	6.002 *(0.021)*	6.008 *(0.036)*	5.924 *(0.035)*	5.999 *(0.024)*
^{T}Al	0.004	0	0.076	0.001
^{Z}Al	6	6	6	6
^{Y}Al	0.772 *(0.089)*	0.448 *(0.127)*	0.500 *(0.040)*	0.655 *(0.053)*
Ti	0.005 *(0.002)*	0.017 *(0.011)*	0.038 *(0.009)*	0.023 *(0.012)*
Cr	0.001 *(0.002)*	0.002 *(0.002)*	0.002 *(0.001)*	0.002 *(0.002)*
Fe^{2+}	1.438 *(0.078)*	1.628 *(0.071)*	1.495 *(0.056)*	1.299 *(0.039)*
Mn	0.002 *(0.002)*	0.003 *(0.003)*	0.003 *(0.003)*	0.001 *(0.002)*
Mg	0.780 *(0.041)*	0.895 *(0.091)*	0.963 *(0.033)*	1.022 *(0.061)*
Ca	0.002 *(0.001)*	0.001 *(0.001)*	0.007 *(0.003)*	0.003 *(0.001)*
Na	0.384 *(0.070)*	0.577 *(0.068)*	0.622 *(0.034)*	0.451 *(0.066)*
K	0.002 *(0.001)*	0.003 *(0.005)*	0.009 *(0.004)*	0.002 *(0.002)*
$^{X}\square$[1]	0.611 *(0.072)*	0.418 *(0.067)*	0.362 *(0.036)*	0.545 *(0.067)*
F	0.007 *(0.006)*	0.020 *(0.026)*	0.021 *(0.018)*	0.010 *(0.000)*
Cl	0.001 *(0.002)*	0.001 *(0.001)*	0.001 *(0.001)*	0.000 *(0.000)*
OH[1]	3.816 *(0.057)*	3.896 *(0.060)*	3.831 *(0.046)*	3.832 *(0.060)*
O[1]	0.176 *(0.057)*	0.083 *(0.060)*	0.147 *(0.046)*	0.158 *(0.060)*
Mg/(Mg+Fe)	0.352 *(0.018)*	0.354 *(0.026)*	0.392 *(0.017)*	0.440 *(0.022)*

[1] Calculated using stoichiometric constraints (see Analytical Techniques).
[2] Numbers in parentheses are standard deviations of the mean (1σ). The standard deviation listed with ^{Y}Al is for total Al.

of the tourmalinite clast has a composition distinct from the acicular pale green-blue generation-3 grains. The average change in composition from the pale green-blue generation-3 tourmaline to that of the gray-blue generation-3 tourmaline is ΔAl = -0.155, $\Delta^{X}\square$ = -0.183, ΔFe = +0.196, ΔMg = +0.059 and ΔNa = +0.171 (Table 4). To understand more fully the proper substitutional trends within each generation of tourmaline, individual data points are plotted on a series of compositional diagrams (Figs. 9-14). For clarity, generation-1 tourmaline is generally plotted on different diagrams than generations-2 and -3 tourmaline.

In terms of general classification based strictly on the X-site occupancy (cf. Hawthorne and Henry, 1999), generation-1 tourmaline is exclusively an alkali group

tourmaline with significant variation between Na and $^{X}\square$, but with very minor incorporation of Ca (Fig. 9a). The pale green zone is slightly enriched in Na compared to the other color zones in generation-1 tourmaline. Generations-2 and -3 tourmalines span the alkali- and vacancy-group tourmalines with the colorless or pale green-blue zones predominantly in the vacancy group (Fig. 9b).

Because all of the tourmalines are aluminous (Al > 6 apfu) and are apparently dominated by OH in the V and W sites (Tables 3 and 4), the best diagram for classification of the tourmaline species is an Mg / (Mg + Fe) vs. X-vacancy / (X-vacancy + Na) diagram (Fig. 10). Generation-1 tourmaline ranges from schorl to dravite [Mg / (Mg + Fe) = 0.27 - 0.61] with the different color zones generally being separated by a distinct range of Mg / (Mg + Fe) (Fig. 10a; Table 2). Within the brown-green and pale-green color zones there is an inverse relation between $^{X}\square$ and X_{Mg}. Generation-2 tourmaline bands exhibit compositional asymmetry as manifest by the blue margins being schorl and the colorless margins being enriched in $^{X}\square$ such that they generally fall in the foitite field (Fig. 10b). In contrast to the generation-1 tourmaline, the trend of increasing $^{X}\square$ is not accompanied by a significant change in X_{Mg} (0.32-0.41) in generation-2 tourmaline (Fig. 10b; Table 4). The generation-3 tourmaline is generally similar to the generation-2 tourmaline with the gray-blue tourmalines being schorl and the pale green-blue tourmaline being schorl-to-foitite (Fig. 10b).

Several of the most important substitutions in each of the tourmaline generations are illustrated by an Al(total) vs. $^{X}\square$ diagram (Fig. 11). Generation-1 tourmaline is clearly separated from generation-2 tourmaline along two nearly subparallel trends with generation-2 tourmaline having uniformly greater $^{X}\square$. A linear least squares fit of the 91 data points from all of the color zone data of the generation-1 tourmaline defines the line $^{X}\square = 0.508$ (Al) - 3.08, with a correlation coefficient of 0.856. The slope of 0.508 implies that most of the Al variations are due to roughly coequal influence by the $\square Al(NaR)_{-1}$ and $AlO(R(OH))_{-1}$ exchange vectors where R is (Fe + Mn + Mg). The 36 generation-2 data points fall along the linear least squares line $^{X}\square = 0.570$ (Al) + 3.28, with a correlation coefficient of 0.964. The slightly steeper slope implies that $\square Al(NaR)_{-1}$ is the more important exchange vector, but that the $AlO(R(OH))_{-1}$ exchange vector still plays a significant role in compositional variation. This is consistent with the magnitude of changes observed in the average values of the zone-1 and zone-2 (generation-2) tourmaline (Table 4). Generation-3 tourmaline falls in two clusters. The gray-blue generation-3 tourmaline generally falls between these the generation-1 and generation-2 trends, but the pale green-blue tourmaline falls near the generation-2 trend.

In addition to Al, the other major variable substituents in the tourmaline are Mg and Fe. To establish whether the Mg-Fe variability is strictly controlled by the simple homovalent substitution $MgFe_{-1}$, Mg vs. Fe diagrams were constructed for each tourmaline generation (Fig. 12). Generation-1 tourmaline generally falls along the reference line that is parallel to the $MgFe_{-1}$ exchange vector, but there are significant deviations from the line. This implies that Fe and Mg do not exclusively substitute for each other, but other substitutions must preferentially incorporate Mg or Fe. Based on the previously-noted positive correlation between $^{X}\square$ and X_{Mg}, Mg is also likely to

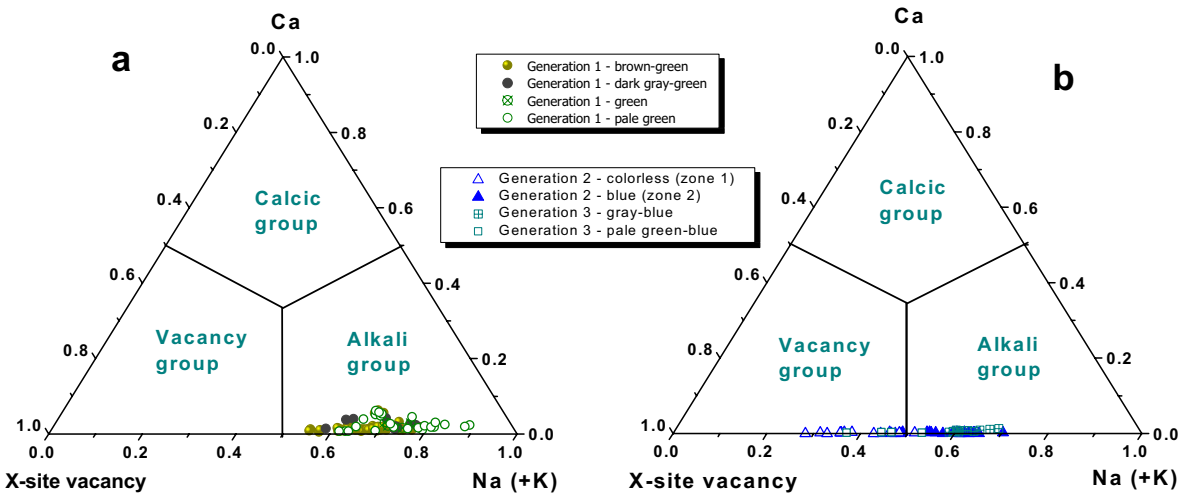

Figure 9. Principal tourmaline groups of the three tourmaline generations based on the classification scheme of Hawthorne and Henry (1999). (a) Generation-1 tourmaline is distinguished by color zones. (b) Generations-2 and -3 tourmalines are distinguished by color zones.

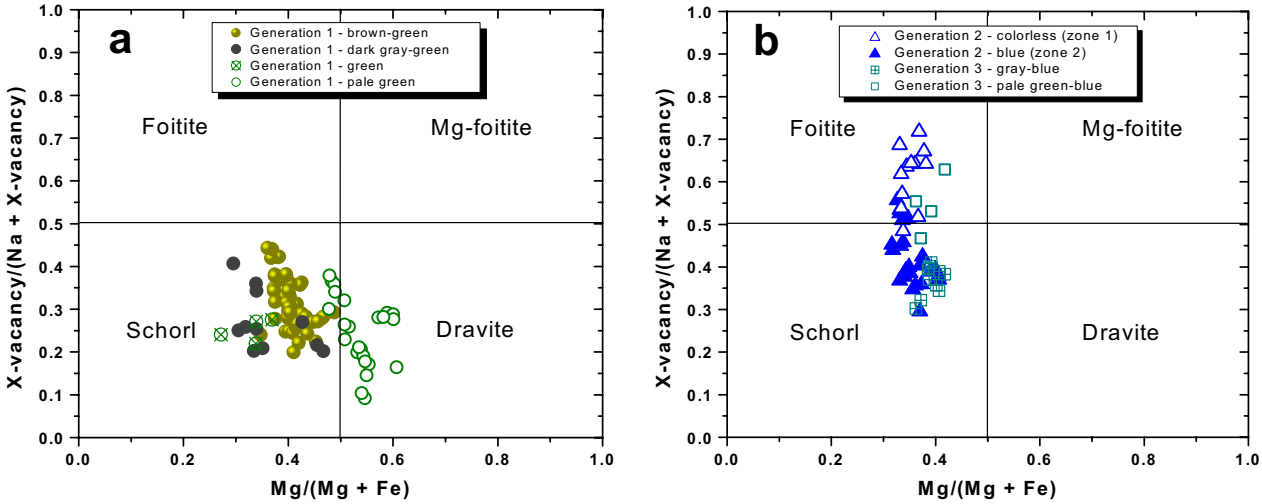

Figure 10. Nomenclature diagram for Al- and OH-dominant tourmaline. (a) Generation-1 tourmaline is distinguished by color zones. (b) Generations-2 and -3 tourmalines are distinguished by color zone.

be substituting in generation-1 tourmaline via the $\square Al(NaMg)_{-1}$ exchange vector. To further test whether the $\square Al(NaMg)_{-1}$ vector primarily accounts for the deviation, the influence of the vector can be removed by adding $^{X}\square$ to Mg i.e. condensing down that vector (Fig. 13) (cf. Burt, 1989; Henry and Dutrow, 1990). The generation-1 tourmaline from the different color zones clusters much more tightly, falling along a line with a least squares regression of Fe = -0.803 (Mg + $^{X}\square$) + 2.39, with a correlation coefficient of –0.952. However, the slope of –0.803 implies that these data still deviate from the $MgFe_{-1}$ exchange vector, most likely reflecting the $AlO(Mg(OH))_{-1}$ exchange vector. Generations-2 and -3 tourmaline data are widely dispersed on the Mg-Fe diagram (Fig. 12b), but if the $\square Al(NaMg)_{-1}$ vector is taken into account, they are clustered along a line with a least squares regression of Fe = -1.242 (Mg + $^{X}\square$) + 3.23, with a correlation coefficient of –0.805 (Fig. 13b). The steeper slope of –1.242 implies that the $MgOH(AlO)_{-1}$ is likely to be the operative exchange vector that produces the deviation from a slope of 1. Because most of the variation in the Fe can be correlated with the substitution of Fe for Mg after taking the $\square Al(NaMg)_{-1}$ and $AlO(Mg(OH))_{-1}$ exchange vectors into account, the assumption of all Fe as Fe^{2+} seems warranted. However, some of the dispersion of the data could be the result of small amounts of Fe^{3+} substituting in accordance with the $FeAl_{-1}$ exchange vector, particularly in the blue zone-1 (generation-2) foitites.

The above arguments suggest that generation-1 tourmaline is enriched in O^{2-} on the W site relative to generations-2 and -3 tourmaline. In a semi-quantitative sense, this can be tested by plotting Al - $^{X}\square$ vs. excess charge (Fig. 14). The excess charge provides a minimum estimate for the replacement of O^{2-} for OH^{-}, albeit with a significant amount of uncertainty. Nonetheless, this plot, together with Tables 3 and 4, indicates that generation-1 tourmaline has a greater amount of O^{2-} for OH^{-} substitution. Interestingly, O^{2-} on the W site tends to induce short range disordering such that more Al occupies the Y site displacing Mg to the Z site (Hawthorne and Henry, 1999). This effectively decouples substitution of Mg so that it does not strictly follow the simple $MgFe_{-1}$ exchange vector. In turn, this probably accounts for the inverse correlation between X_{Mg} and $^{X}\square$ observed in generation-1 tourmaline (Fig. 10a).

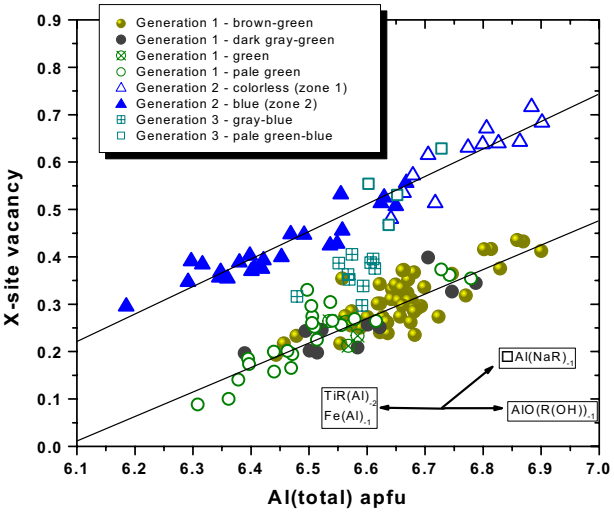

Figure 11. Al(total) vs. X-site vacancy for all generations of tourmaline. The solid lines are separate least squares fits to the generations-1 and -2 data. The directions of several selected exchange vectors are shown for reference.

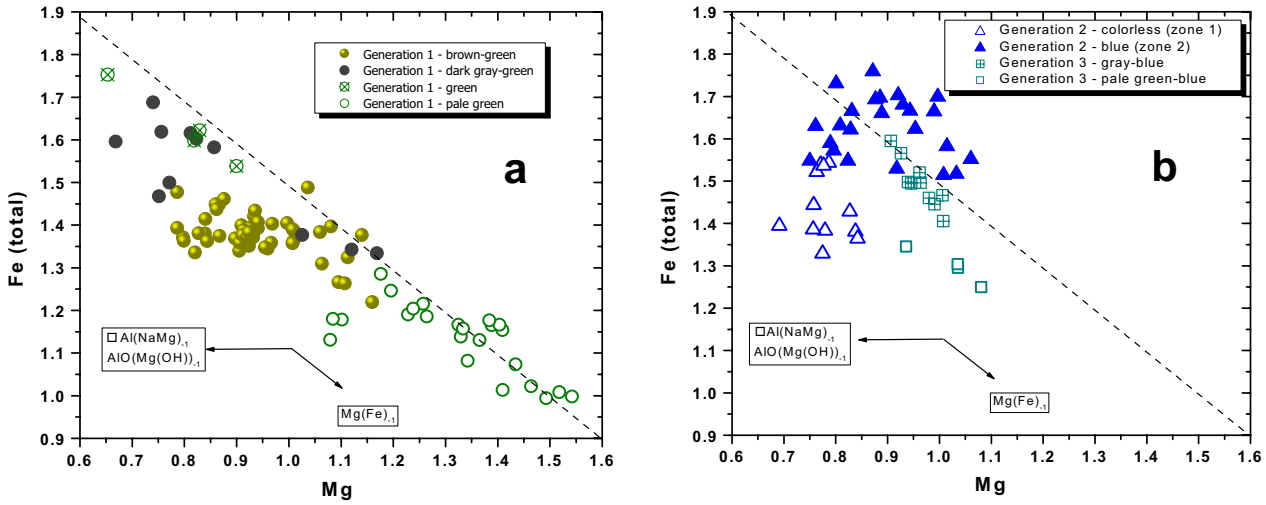

Figure 12. Mg vs. Fe(total) for all generations of tourmaline. (a) Generation-1 tourmaline is distinguished by color zones. (b) Generations-2 and -3 tourmalines are distinguished by color zone. The dashed lines are reference lines with a slope of –1, parallel to the Mg(Fe)$_{-1}$ exchange vector. The directions of several selected exchange vectors are shown for reference.

Discussion

Textural and compositional data of tourmaline and associated minerals give an insight into the genesis of this tourmaline-bearing rock. Each tourmaline generation allows a glimpse into the thermal, deformational and fluid evolution experienced by this rock during distinct episodes of geologic history of the Tauern Window. Furthermore, the nature of the generation-2 replacement tourmaline reveals a style of compositional asymmetry in tourmaline that is distinctly different from that of compositional polarity.

Generation-1 tourmalinite development

The origin of the quartz + tourmaline vein is difficult to precisely establish, but there are several observations that bear on its development. The bulk compositions of lazulite-bearing Permo-Triassic quartzites, host of the tourmalinite vein, are generally characterized by high Al, P, F, B, U, Th and low Na relative to normal muscovite-bearing quartzites (Morteani and Ackermand, 1996). These aluminous metasediments are interpreted as originally being sabkha-like sediments. A hydrothermal vein cutting through, and interacting with, the original aluminous metasedimentary rock will acquire some of the geochemical characteristics of that rock. The relatively large amount of apatite in the tourmalinite clast probably reflects the P-enriched host rock.

The quartz + tourmaline veins may represent mobilization of B originating from nearby evaporative sequences, or they may be due to completely separate external fluid. The relatively coarse grain size of the generation-1 tourmaline is consistent with tourmalinite development above zeolite facies conditions (Slack, 1996). The heterogeneous and locally oscillatory nature of the generation-1 tourmaline further suggests an open, dynamic hydrothermal environment of crystallization (cf. Slack, 1996; London et al., 1996). These generation-1 textures are not likely to have been modified by volume diffusion even at the peak thermal conditions of 550°C, and probably represent the primary zoning characteristics of the tourmaline (Henry and Dutrow, 1996). Furthermore, the blue-luminescent quartz inclusions in the generation-1 tourmaline represent an earlier generation of quartz, likely with relatively elevated Ti and/or Al contents. CL images establish that red-luminescent quartz recrystallized after deformation and presumably released the Ti and/or Al during recrystallization. Because the veins crosscut bedding, vein emplacement clearly postdated Permo-Triassic deposition of the quartzite protolith, and because the vein is deformed by shearing, vein emplacement predated shearing and subsequent Alpine peak thermal metamorphism (~30 Ma).

The textural and compositional variability of the complex color zones developed in generation-1 tourmaline provides clues about the fluids that must have been present during the original formation of the tourmalinites. Some of the dark gray-green generation-1 tourmaline patches crosscut the textural features associated with lighter brown-green and green zones. This implies that an earlier stage(s) of replacement took place during the crystallization of generation-1 tourmaline. There is variable X_{Mg} [Mg / (Mg + Fe) = 0.27 - 0.61] in the different zones, likely reflecting differential influx of these constituents in the fluid during growth. The relatively high Al content in the generation-1 tourmaline is believed to reflect the relatively aluminous bulk composition of the host quartzite. However, the highly variable Al contents

in the generation-1 tourmaline are most likely controlled by factors relating to the fluid phase. The $\square Al(NaR)_{-1}$ and $AlO(R(OH))_{-1}$ exchange vectors are roughly coequal in accounting for the variable Al in generation-1 tourmaline. Because the $\square Al(NaR)_{-1}$ and $AlO(R(OH))_{-1}$ exchange vectors in tourmaline are influenced by the Na contents in coexisting aqueous fluids (von Goerne et al., 2001) and pH, respectively, the Al variability in the generation-1 tourmaline can be largely explained by variable fluid-rock reactions during dynamic tourmalinite formation. Furthermore, based on the general characteristics of the primary three-phase fluid inclusions in generation-1 tourmaline, CO_2 is also an important component of the tourmalinite-forming fluid phase.

Generation-2 tourmaline and reactive fluids

Fractures developed in the tourmalinite are due to regional stresses, with the host quartzite and tourmalinite vein being strongly tectonized within the subvertical Greiner shear zone, a structure considered to have developed during the Alpine orogeny (e.g. Selverstone, 1993). Most of the deformation within the Greiner shear zone of the Lower Schieferhülle occurred prior to attainment of T_{max}, and its attendant post-deformational porphyroblast growth and recrystallization at ~ 30 Ma (Selverstone, 1985, 1993). This sets the likely time for generation-1 tourmaline fracturing and introduction of reactive fluids to be during the earlier part of the Alpine orogeny.

The distinctive compositional asymmetry exhibited by generation-2 tourmaline reflects the interplay between reactive metamorphic fluids and the tourmaline replacement process. The generation-2 tourmaline is optically continuous with generation-1 tourmaline indicating a crystallographically-controlled replacement process. Colorless bands of zone-1 foitite apparently replace generation-1 tourmaline along scalloped replacement fronts that advance preferentially towards the -c end of generation-1 tourmaline. Replacement of the generation-1 tourmaline host in this manner is similar to natural and experimental etching that results in more rapid dissolution in the direction of the analogous pole, -c direction, of tourmaline (e.g. Krynine, 1946; Wooster, 1976; Dietrich, 1985). The blue zone-2 bands of generation-2 tourmaline develop as acicular schorl crystals that intergrow with, and partially replace, zone-1 foitite (Fig. 8). Based on stability experiments, it is known that tourmaline is generally destabilized under alkaline conditions, in part due to the enhanced concentration of Al in solution (Frondel and Collette, 1957; Morgan and London, 1989; London et al., 1996). Furthermore, experiments involving quartz + tourmaline assemblages demonstrate that the amount of Na in the X-site of tourmaline is a function of both temperature and Na content of a coexisting aqueous fluid phase (von Goerne et al., 2001). Specifically, at constant temperature the Na content of tourmaline increases with increasing Na concentration in the fluid, whereas at constant Na concentration in the fluid the Na content in the tourmaline should decrease as the temperature increases. Consequently, the general compositional changes from generation-1 to generation-2 tourmaline of lower Na and higher OH (Figs. 10, 14) are most consistent with an influx of an initial reactive

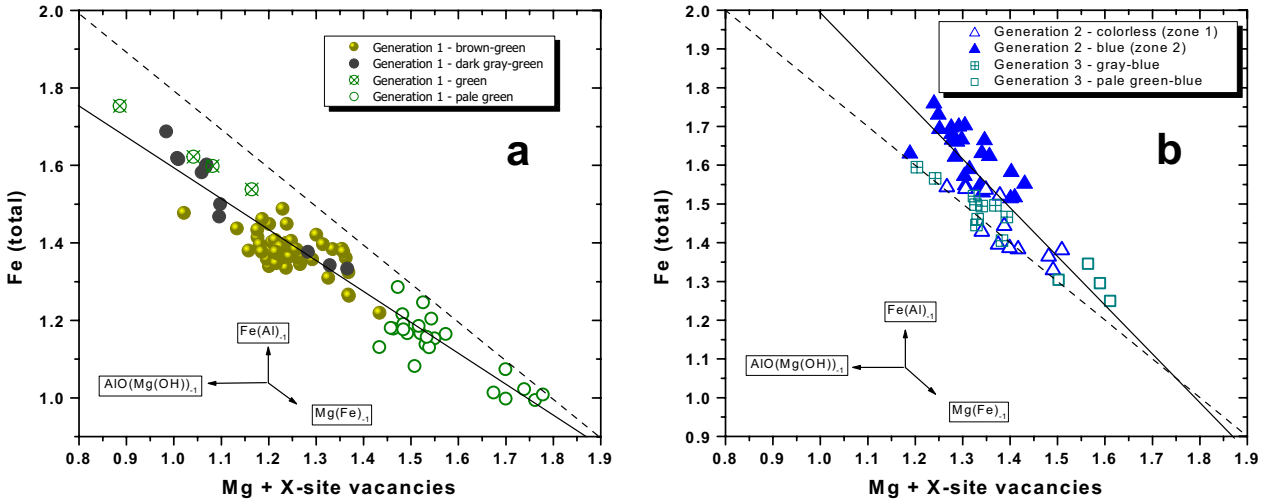

Figure 13. Mg + X-site vacancies vs. Fe(total) for all generations of tourmaline. The addition of X-site vacancies to Mg results in the condensation of the data down the $\square Al(NaMg)_{-1}$ exchange vector. (a) Generation-1 tourmaline is distinguished by color zones. (b) Generations-2 and -3 tourmalines are distinguished by color zone. The dashed lines are reference lines with a slope of –1, parallel to the $Mg(Fe)_{-1}$ exchange vector. The solid lines are least squares fits to the generation-1 data in (a) and generation-2 data in (b).

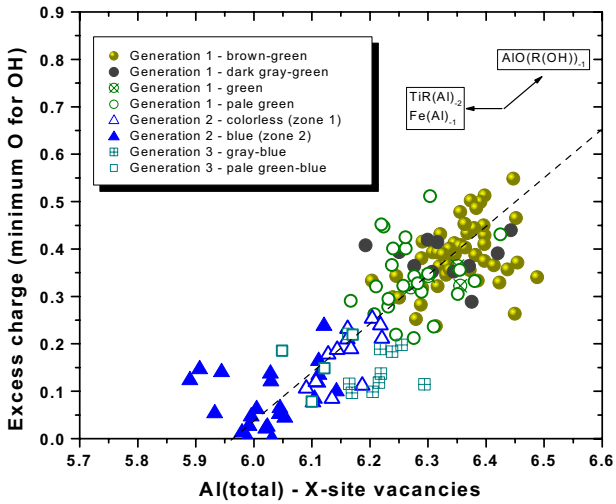

Figure 14. Al – X-site vacancies vs. excess charge for all generations of tourmaline. Excess charge is a measure of the minimum replacement of O^{2-} for OH^-. Subtraction of X-site vacancies from Al results in condensation of the data down the $\square Al(NaR)_{-1}$ exchange vector. The dashed line is a reference line with a slope of 1, parallel to the $AlO(R(OH))_{-1}$ exchange vector.

neutral-to-alkaline, low-Na fluid phase, possibly accompanied by an increase in temperature.

Growth of the zone-1 foitite and zone-2 schorl could have been sequential or simultaneous, depending on the interpretation of the textures. (1) If the partial crosscutting of zone-1 growth features by the zone-2 acicular crystals are interpreted as signaling a sequential development of foitite followed by schorl, it might be argued that the reactive fluids fractionates with progressive replacement of generation-1 tourmaline. Zone-2 schorl could have been formed at the expense of zone-1 foitite if the residual fluid at the fracture became slightly more alkaline and enriched in Fe and Na, possibly as a result of Fe and Na released by foitite replacement of generation-1 tourmaline. The development of foitite with subsequent replacement by schorl in generation-2 tourmaline is a relatively common phenomenon in dynamic hydrothermal environments. Tourmaline fibers that partially replace pegmatitic elbaite from the Cruzeiro Mine, Brazil are complexly-zoned with four distinct generations marked by discrete compositions and replacement textures punctuated by periods of dissolution (Dutrow and Henry, 2000). The compositional changes associated with the first three generations of fiber growth from foitite to schorl to "fluor-elbaite" are considered to represent a fractionation trend of the orthomagmatic/hydrothermal fluids. Fibrous overgrowths of foitite have been found nucleating on pegmatitic schorls and elbaites from Elba (Pezzotta et al., 1996; Aurisicchio et al., 1999). Aurisicchio et al. (1999) note that foitite probably developed during a zeolitic hydrothermal stage associated with localized microfractures and later schorlitic overgrowths are associated with a later hydrothermal fluid transects the monzogranite such that it produced an open hydrothermal system. (2) If there was a single pulse of reactive fluid, the progressive replacement zoning could be interpreted as a solid state reaction associated with intracrystalline diffusion to produce the observed compositional changes. The concentration of fluid inclusions near the fracture and the paucity of fluid inclusions at the colorless replacement front are consistent with this interpretation. Cesare and Gobéty (1995) note that replacement of kyanite by staurolite takes place by spikes or lamellae of the replacing phase projecting within the unstable phase. If the replacement zoning is controlled by intracrystalline diffusion the style of zoning will be controlled by the least mobile species, probably Al (cf. Cesare and Grobéty, 1995). However, the discontinuity in the compositions from zone1 to zone 2 suggests that simple diffusional replacement does not completely explain the compositional patterns. Ultimately, elements of both the fluid fractionation and solid-state diffusional mechanisms may be operative.

Generation-3 tourmaline

Generation 3 tourmaline is post-deformational and has minor compositional zoning. This tourmaline generation probably developed during the peak thermal metamorphism at roughly the same time as post-kinematic kyanite and lazulite porphyroblasts i.e. at ~30 Ma. Compositionally, the generation-3 tourmalines are similar to generation-2 tourmalines, and likely reflect similar fluid compositions. The peak metamorphic fluid compositions in this sample are not known with certainty. However, isolated fluid inclusions in the cores of quartz grains of veins in adjacent outcrops are relatively CO_2-rich with $X(CO_2)$ of 0.4-0.5 and 4-11 wt% NaCl in the aqueous fluid inclusions (Selverstone et al., 1995). These fluid inclusions are considered to contain fluids representative of peak thermal metamorphic conditions. Further delineation of fluid compositions awaits detailed fluid inclusion investigations of the tourmalinite.

Compositional asymmetry in tourmaline

The compositional asymmetry due to replacement is distinctly different than the style of compositional asymmetry exhibited by tourmaline with compositional polarity features. Tourmalines that exhibit compositional polarity concurrently develop disparate compositions at the opposite poles of the tourmaline crystal such that the tourmaline developed at the +c end is typically more aluminous and enriched in X-site vacancies relative to tourmaline developed at the –c end of the tourmaline crystal. This phenomenon is largely related to differential surface energies at disparate faces in tourmaline and is, consequently, most pronounced at low temperatures (Henry and Dutrow, 1992, 1996; Henry et al., 1999).

In contrast, the compositional asymmetry associated with replacement, as observed in this study, takes place preferentially in the direction of the -c end of the host tourmaline. The compositional asymmetry is manifest by the most foititic tourmaline forming at the replacement front and acicular schorl developing proximal to a fracture or grain boundary. Replacement implies selective removal of cations while leaving others. It is a process of opening the chemical system to accept and eliminate materials involved in chemical change. The composition of the generation-2 tourmaline and mechanism of replacement are controlled by phenomena at the host tourmaline/replacement phase interface, within the replacing phase and in the reactive fluid. Whether the replacement mechanism is related to fractionating reactive fluid and/or solid-state diffusion in the tourmaline, the result is a production of tourmaline that exhibits distinctive compositional asymmetry.

Acknowledgements

We would like to acknowledge Xiaogang Xie for assistance with microanalysis and image analysis. This work was supported by NSF grant EAR-9405747 to DJH and NSF grant EAR-9814418 to BLD. We thank Bernardo Cesare, John Brady, Milan Novák and Yves Fuchs for insightful and careful reviews.

References Cited

Aurisicchio, C., DeMartin, F., Ottolini, L., and Pezzotta, F. (1999) Homogeneous liddicoatite from Madagascar: a possible reference material? First EMPA, SIMS and SREF data. European Journal of Mineralogy, 11, 237-242.

Barton, P. Jr. (1969) Refinement of the crystal structure of buergerite and the absolute orientation of tourmalines. Acta Crystallographica, B25, 1524-1533.

Bruhn, F., Bruckshen, P., Meijer, J., Stephan, A., Richter, D.K., and Veizer, J. (1996) Cathodoluminescence investigations and trace-element analyses of quartz by micro-PIXE: implications for diagenetic and provenance studies in sandstones. Canadian Mineralogist, 34, 1223-1232.

Burt, D.M. (1989) Vector representation of tourmaline compositions. American Mineralogist, 74, 826-839.

Cesare, B. and Grobéty, B. (1995) Epitaxial replacement of kyanite by staurolite: A TEM study of microstructures. American Mineralogist, 80, 78-86.

Christensen, J., Selverstone, J., Rosenfeld, J., and DePaolo, D. (1994) Correlation by Rb-Sr geochronology of garnet growth histories from different structural levels within the Tauern Window, Eastern Alps. Contributions to Mineralogy and Petrology, 118, 1-12.

Craig, J.R. and Vaughan, D.J. (1994) Ore Microscopy and Ore Petrography. Second Edition, John Wiley and Sons, New York.

Dietrich, R.V. (1985) The Tourmaline Group. Van Nostrand Reinhold Co. New York.

Dutrow, B.L., Holdaway, M.J., and Hinton, R.W. (1986) Lithium in staurolite and its petrologic significance. Contributions to Mineralogy and Petrology, 94, 496–506.

Dutrow, B.L., Foster, C.T., Jr., and Henry, D.J. (1999) Tourmaline-rich pseudomorphs in sillimanite zone metapelites: Demarcation of an infiltration front. American Mineralogist, 84, 794-805.

Dutrow, B. and Henry, D.J. (2000) Complexly zoned fibrous tourmaline: A record of evolving magmatic and hydrothermal fluids. Canadian Mineralogist, 38, 131-143.

Frondel, C. and Collette, R L. (1957) Synthesis of tourmaline by reaction of mineral grains with NaCl-H_3BO_3 solution, and its implications in rock metamorphism. American Mineralogist, 42, 754-758.

Hawkins, K.D., Mackinnon, I.D.R., and Schneeberger, H. (1995) Influence of chemistry on the pyroelectric effect in tourmaline. American Mineralogist, 80, 491-501.

Hawthorne, F.J. and Henry, D.J. (1999) Classification of the minerals of the tourmaline group. European Journal of Mineralogy, 11, 201-216.

Henry, D.J. and Dutrow, B.L. (1990) Ca substitution in Li-poor aluminous tourmaline, Canadian Mineralogist, 28, 111-124.

Henry, D.J. and Dutrow, B.L. (1992) Tourmaline in a low grade clastic metasedimentary rocks: an example of the petrogenetic potential of tourmaline: Contributions to Mineralogy and Petrology, 112, 203-218.

Henry, D.J. and Dutrow, B.L. (1996) Metamorphic Tourmaline. In: E.S. Grew and L.M. Anovitz (Editors), Boron: Mineralogy, Petrology and Geochemistry. Reviews in Mineralogy. 33, 500-555.

Henry, D.J. and Dutrow, B. (2001) Compositional zoning and element partitioning of nickeloan tourmaline in a metamorphosed karstbauxite from Samos, Greece. American Mineralogist, 86, 1130-1142.

Henry, D.J. and Guidotti, C.V. (1985) Tourmaline as a petrogenetic indicator mineral: an example from the staurolite-grade metapelites of NW Maine. American Mineralogist, 70, 1-15.

Henry, D.J., Kirkland, B.L., and Kirkland, D.W. (1999) Sector-zoned tourmaline from the cap rock of a salt dome. European Journal of Mineralogy, 11, 263-280.

Krynine, P.D. (1946) The tourmaline group in sediments. Journal of Geology, 54, 65-87.

Kurz, W., Neubauer, F., and Dachs, E. (1998) Eclogite meso- and micro-fabrics: implications for the burial and exhumation history of eclogites in the Tauern Window (Eastern Alps) from P-T-d paths. Tectonophysics, 285, 183-209.

London, D. (1999) Stability of tourmaline in peraluminous granite systems: the boron cycle from anatexis to hydrothermal aureoles. European Journal of Mineralogy, 11, 253-262.

London, D., Morgan, G.B. IV, and Wolf, M.B. (1996) Boron in granitic rocks and their contact aureoles. In: E.S. Grew and L.M. Anovitz (Editors), Boron: Mineralogy, Petrology and Geochemistry. Reviews in Mineralogy. 33, 299-330.

Matter, A. and Ramseyer, K. (1985) Cathodoluminescence microscopy as a tool for provenance studies of sandstones. In Zuffa, G. G., editor, Provenance of Arenites, NATO ASI Series, 148, 191-211.

Morgan, G.B. IV and London, D. (1989) Experimental reactions of amphibolite with boron-bearing aqueous fluids at 200 MPa: implications for tourmaline stability and partial melting in mafic rocks. Contributions to Mineralogy and Petrology, 102, 281-297.

Morteani, G. (1974) Petrology of the Tauern Window, Austrian Alps. Fortschriftte Mineralogische, 52, 195-220.

Morteani, G. and Ackermand, D. (1996) Aluminum phosphates in muscovite-kyanite metaquartzites from Passo di Vizze (Alto Adige, NE Italy). European Journal of Mineralogy, 8, 853-869.

Novák, M. (1998) Blue dravite as an indicator of fluid composition during subsolidus replacement processes in Li-poor granitic pegmatites in the Moldanubicum, Czech Republic, Journal of the Czech Geological Society, 43, 24-30.

Perny, B., Eberhardt, P., Ramseyer, K., Mullis, J., and Pankrath, R. (1992) Microdistribution of Al, Li, and Na in a quartz: Possible causes and correlation with short-lived cathodoluminescence. American Mineralogist, 77, 534-544.

Pezzotta, F., Hawthorne, F.C., Cooper, M.A., and Teertstra, D.K. (1996) Fibrous foitite from San Piedro. Canadian Mineralogist, 34, 741-744.

Selverstone, J. (1985) Petrologic constraints on imbrication, metamorphism, and uplift in the SW Tauern Window, eastern Alps. Tectonics, 4, 687-704.

Selverstone, J. (1993) Micro- to macro-scale interactions between deformation and metamorphism, Tauern Window, Eastern Alps. Schweizerische Mineralogische Petrographische Mitteilungen, 73, 229-239.

Selverstone, J. and Munoz, J.L. (1987) Fluid heterogeneities and hornblende stability in interlayered graphitic and nongraphitic schists (Tauern Window, Eastern Alps), Contributions to Mineralogy and Petrology, 96, 426-440.

Selverstone, J., Axen, G.J., and Bartley, J.M. (1995) Fluid inclusion constraints on the kinematics of footwall uplift beneath the Brenner Line normal fault, eastern Alps. Tectonics, 14, 264-278.

Selverstone, J., Morteani, G., and Staude, J.-M. (1991) Fluid channeling during ductile shearing: transformation of granodiorite into aluminous schist in the Tauern Window, Eastern Alps. Journal of Metamorphic Geology 9, 419-431.

Selverstone, J., Spear, F.S., Franz, G., and Morteani, G. (1984) High-pressure metamorphism in the SW Tauern Window, Austria: P-T paths from hornblende-kyanite-staurolite schists. Journal of Petrology, 25, 501-531.

Slack, J.F. (1996) Tourmaline associations with hydrothermal ore deposits. In: E.S. Grew and L.M. Anovitz (Editors), Boron: Mineralogy, Petrology and Geochemistry. Reviews in Mineralogy. 33, 559-644.

Smith, A.G. and Woodcock, N.H. (1982) Tectonic syntheses of the Alpine-Mediterranean region: A review. In H. Berckheimer and K. Hsu, editors, Alpine-Mediterranean Geodynamics, American Geophysical Union, Washington, D.C., 15-38.

Sperlich, R., Giere, R., and Frey, M. (1996) Evolution of compositional polarity and zoning in tourmaline during prograde metamorphism of sedimentary rocks in the Swiss Central Alps. American Mineralogist, 81, 1223-1236.

Srein, V., Litochleb, J., Sjkora, J. Sreinova, B., and Pivec, E. (1997): Fibrous dravite from quartz lode near Krasovice in central Bohemia. Tourmaline 1997, International Symposium on Tourmaline, Abstract Volume, 99-100.

von Blanckenburg, F., Villa, I.M., Morteani, G., and Steiger, R.H. (1989) Time calibration of a PT-path from the western Tauern Window, Eastern Alps. Contributions to Mineralogy and Petrology, 101, 1-11.

von Goerne, G., Franz, G., and Heinrich, W. (2001) Synthesis of tourmaline solid solutions in the system Na_2O-MgO-Al_2O_3-SiO_2-B_2O_3-H_2O-HCl and the distribution of Na between tourmaline and fluid at 300 to 700 ˚C and 200 MPa. Contributions to Mineralogy and Petrology, 141, 160-173.

Walderhaug, O. and Rykkje, J. (2000) Some examples of the effects of crystallographic orientation on the cathodoluminescence colors of quartz. Journal of Sedimentary Research, 70, 545-548.

Werding, G. and Schreyer, W. (1996) Experimental studies on borosilicates and selected borates. In: E.S. Grew and L.M. Anovitz (Editors), Boron: Mineralogy, Petrology and Geochemistry. Reviews in Mineralogy. 33, 117-163.

Wooster, W.A. (1976) Etch figures and crystal structures. Kristall und Technik, 11, 615-623.

Zinkernagel, U. (1978) Cathodoluminescence of quartz and its application to sandstone petrology. Contributions to Sedimentology, 8, 1-69.